PHILOSOPHICAL TRANSACTIONS OF THE ROYAL SOCIETY A

Phil. Trans. R. Soc. A (2008) **366**, 2131–2143
doi:10.1098/rsta.2008.0003
Published online 18 March 2008

The role of feedback in microfluidic flow-focusing devices

By Matthew T. Sullivan[1,2] and Howard A. Stone[1,*]

[1]*School of Engineering and Applied Sciences, Pierce Hall, Harvard University, 29 Oxford Street, Cambridge, MA 02138, USA*
[2]*Schlumberger-Doll Research, 1 Hampshire Street, Cambridge, MA 02139, USA*

A model was developed for the analysis of steady and unsteady bubble generation frequencies in a microfluidic flow-focusing device. In both cases, the generation frequency depends on the downstream influence of bubbles created by the flow-focusing device, which provides a source of feedback. For steady-state generation of bubbles, this feedback explains the relationships among frequency, gas pressure and liquid flow rate in our experiments as well as gives a physical explanation for previously observed frequency relations. The role of feedback is also exploited to explain unsteady behaviour; we develop a numerical model and analytical expressions that agree with experimental measurements.

Keywords: microfluidics; flow focusing; feedback

1. Introduction

A wide variety of microfluidic devices are available to produce well-controlled and monodisperse foams, emulsions and even multiple emulsions, with volume fractions of the dispersed phase varying from 0 to 1 (see Umbanhowar *et al.* 2000; Ganan-Calvo & Gordillo 2001; Anna *et al.* 2003; Garstecki *et al.* 2004; Okushima *et al.* 2004; Utada *et al.* 2005). The increased control of these flows comes at a cost—system volume throughputs are significantly smaller than with conventional devices. For many applications of microfluidics, such as those in biology and medicine, the decreased volume is beneficial, since it reduces the required amount of expensive protein or reagent (see the review by Beebe *et al.* 2002). To create industrially useful amounts of foam or emulsion, however, the volumetric flow rates produced by microfluidic devices must be increased.

One route to produce larger quantities from microfluidic devices is to run them in parallel. Designing massively parallel microfluidic channels is easy using current fabrication techniques, but the behaviour of microfluidic devices under highly parallel operation is poorly understood. Generating monodisperse foams and emulsions in parallel systems has proved challenging, in part due to the significant crosstalk and feedback in these systems (see, for instance, Barbier *et al.* 2006).

* Author for correspondence (has@seas.harvard.edu).

One contribution of 11 to a Theme Issue ‘New perspectives on dispersed multiphase flows’.

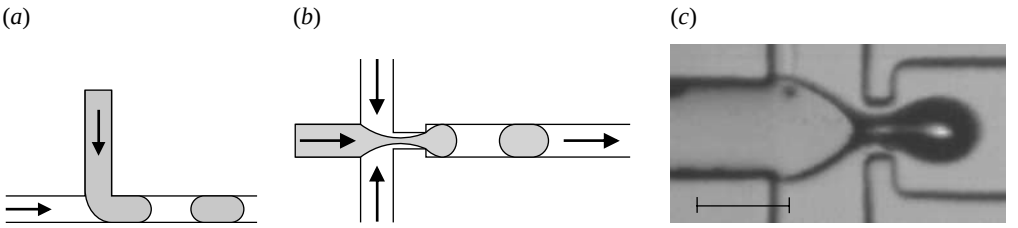

Figure 1. (*a*) Schematic of a T-junction. The discrete phase is injected perpendicular to the continuous phase and is sheared off to produce droplets. (*b*) Schematic of a flow-focusing junction. The discrete phase is injected into a coflowing continuous phase. At the flow-focusing junction, there can be a narrow constriction to focus the flow. (*c*) A typical flow-focusing junction is used in this work, with gas injected into a liquid phase. The width of the input and output channels is 100 μm. The width at the flow-focusing constriction ranges from 25 to 50 μm. The height of all channels is 40 μm. Beyond the junction, the channel continues undeviated for 4 cm before the fluids exit at atmospheric pressure into a waste container. The scale bar is 100 μm.

The primary focus of studies on the generation of multiphase flows is on the dynamics at the fluid–fluid interface. This viewpoint is understandable, as the mechanics of thread break up is an old and fundamentally interesting problem (see the review by Eggers 1997). However, understanding how these devices will operate in parallel requires a complete description of the device, from fluid inlets to multiphase outlet. This approach is especially true for parallel systems, where an increased resistance in one channel can affect the flow rates in all of the other channels.

We use the specific example of a microfluidic flow-focusing bubble generator to demonstrate the interrelation between the behaviour at the fluid–fluid interface and the downstream flow behaviour, including steady-state and time-dependent behaviours. We start by giving a brief review of the principles of multiphase flow generation in microfluidic devices, in particular the behaviour at the fluid–fluid interface. Next, we describe experiments performed to quantify the relationship between the generation frequency of individual drops and the input flow parameters in a flow-focusing device. Remarkably, the generation frequency even in this simple device depends both on the dynamics at the fluid–fluid interface and on the resulting multiphase flow generated from the device. A quantitative theory is developed for the bubbling frequency as a function of the flow and geometrical parameters.

2. Multiphase flow generation

The underlying principle in all microfluidic flow-focusing generators is the injection of one phase, the discrete phase, into a second, immiscible continuous phase. The two most common microfluidic implementations of this idea are the T-junction (see Thorsen *et al.* 2001), where the discrete phase is injected perpendicular to the continuous phase (figure 1*a*), and the flow-focusing junction (see Ganan-Calvo & Gordillo 2001; Anna *et al.* 2003), where the discrete phase is injected into a coflowing continuous phase (figure 1*b*).

The dynamics underlying both the T-junction and flow-focusing devices are controlled by competing stresses—surface tension, pressure, viscous and inertial—at the fluid–fluid interface. As the flow-focusing geometry lends itself to more straightforward experimental, numerical and theoretical description, we

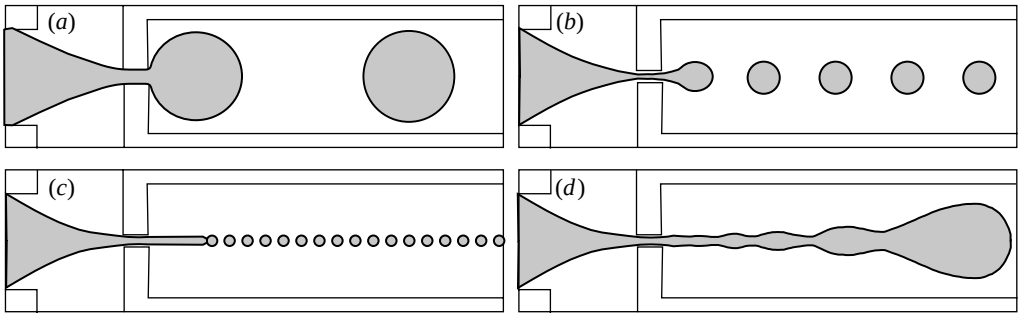

Figure 2. Varieties of different regimes were observed in droplet formation in flow-focusing devices. (*a*) Geometrically controlled break up, (*b*) dripping, (*c*) 'narrowing jetting', and (*d*) 'widening jetting'. Garstecki *et al.* (2004) studied (*a*) geometrically controlled break up and found that droplet formation was controlled by blockage of the constriction and the downstream channel by the discrete phase, which subsequently causes increased pressure behind the constriction and break up of the droplet. (*b*) Dripping is qualitatively similar to geometrically controlled break up, except that pinch-off is not controlled by blockage of the constriction, but instead by viscous drag on the gas thread. In both (*a*,*b*), the inner phase is observed to grow from a minimum size, form a thinning neck behind a leading drop, pinch-off, and finally retract to the original minimum. Stable and unstable jetting occur when a long, thin thread forms and subsequently breaks up due to capillary instabilities. These regimes have been described by Anna & Mayer (2006) in planar geometries and Utada *et al.* (2007) in cylindrical geometries.

focus on the behaviour of these devices, although significant progress has also been made in understanding the operation of T-junction devices (for instance Garstecki *et al.* 2006).

Anna & Mayer (2006) described three distinct regimes in the formation of multiphase flows in planar flow-focusing devices, in the order of increasing capillary number: geometrically controlled break up, dripping, and jetting (figure 2). Garstecki *et al.* (2005) showed that controlled break up occurs when the thread of the discrete phase is comparable in diameter to the flow-focusing constriction. The thread grows until it blocks flow by the continuous phase, at which point the break up of the thread is mediated by volumetric contraction of the thread until pinch-off. The thread then retracts to its original position and the process repeats. Droplets formed in this regime are similar in size to the constriction and are highly monodisperse. Dripping is similar to geometrically controlled break up, except that the break up is not directly controlled by the geometry of the constriction, but instead driven by surface tension (see Eggers 1993).

Jetting is characterized by steady droplet formation and pinch-off from a thread that is significantly smaller and extends considerably further than the flow-focusing junction. Here, break up is controlled by a Rayleigh–Plateau-like capillary instability of the long, thin thread (see Plateau 1849; Lord Rayleigh 1879). Utada *et al.* (2007) found two different regimes of jetting, 'narrowing jetting' and 'widening jetting', characterized by the downstream width of the narrow thread. The narrowing jetting features a jet that narrows downstream of the constriction and the subsequent droplet sizes are comparable to the thread size. The widening jetting is characterized by an increasing width of the thread downstream from the flow-focusing junction, which produces relatively large, polydisperse droplets.

Table 1. Glycerol–water solutions with Tween-20 surfactant.

glycerol wt (%)	surfactant wt (%)	viscosity (mPa s)
71	0.1	19.2
60	0.1	8.7
53	0.1	5.8

3. Steady bubble generation

(a) *Experimental set-up and measurements*

Flow-focusing devices (figure 1*c*) are fabricated in polydimethylsiloxane (PDMS) using standard soft lithography techniques following Duffy *et al.* (1998). We use solutions of glycerol and water combined with Tween-20 surfactant (0.1% wt) as the continuous phase. The solution viscosity is adjusted by changing the relative concentrations of glycerol and water (table 1). The liquid flow rate is controlled using a syringe pump. We use compressed air that is controlled by a pressure regulator as the discrete phase.

Measurements are taken on an inverted microscope using a fast camera, with a typical frame rate of 4000 frames s^{-1}. Analysis of these movies is performed using image analysis software to first find the bubble size and position in each movie frame and then stitch positions together to produce complete tracks for each bubble. From the evolution of bubble position and size with time, all of the relevant parameters for the bubble are calculated. For example, the velocity is measured by using the numerical derivative of the bubble position with respect to time and the frequency is calculated from the time delay between successive bubbles to pass a fixed reference point in the channel. Finally, the volume is estimated as the product of the visible area of the bubble and the height of the channel, since the discrete phase is shaped similar to a disc.

(b) *Experimental results*

The bubble velocity (figure 3) is observed to be approximately equal to the average fluid velocity. For large bubbles in a circular channel, Bretherton (1961) found that the discrepancy between the average fluid velocity and bubble velocity is expected to be proportional to $Ca^{2/3}$, where $Ca = \eta u/\gamma$ is the ratio of viscosity η and velocity u to surface tension γ. While the channel is not circular in cross section in our system, the bubbles are large enough to be geometrically confined along the vertical dimension and produce a thin wetting layer, so this analysis is not entirely inappropriate. A generalization to account for the rectangular cross section and the motion of large bubbles has been given by Wong *et al.* (1995), and confirms this idea.

The steady-state production of bubbles in such a device is characterized by two parameters—the volume of each bubble and the frequency of generation. The bubble volume has been studied experimentally by Garstecki *et al.* (2004) in a planar device and numerically by Jensen *et al.* (2006) for the case of a low Reynolds number axisymmetric flow. In both of these studies, volume was found to be proportional to gas pressure P and inversely proportional to liquid flow rate

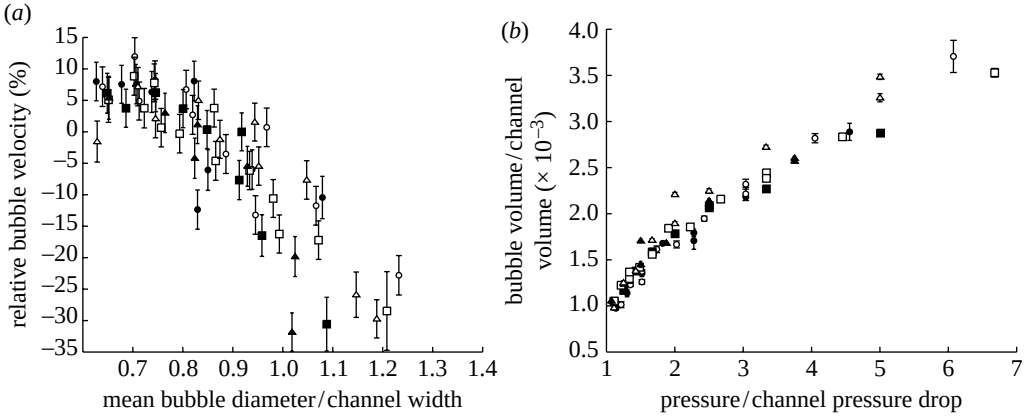

Figure 3. (*a*) Deviation of measured bubble velocity from mean fluid velocity. Deviations from the mean fluid velocity are observed to be proportional to the size of the bubble—large bubbles move slower than the mean fluid and small bubbles move faster. These deviations are generally small for the bubble sizes considered in this work. Fuerstman *et al.* (2007) found significant deviations for bubbles much longer than those considered here. (*b*) Observed bubble volume V_b normalized by the channel volume V_c plotted against gas pressure P normalized by the channel hydrodynamic pressure drop P_c (defined in the text). Garstecki *et al.* (2004) found a linear relation between these two quantities, $V_b = V_t P/P_c$, where V_t is the proportionality constant in the relationship and can be thought of as the volume of the gas thread. Deviations from a directly linear relationship are most likely due to pinch-off before the pressure-controlled bubble growth regime is reached. Such a deviation was observed in a numerical study by Jensen *et al.* (2006), and predominates for small bubbles. In our experiments, we found $V_t \approx 6 \times 10^4\ \mu m^3$, or approximately 60% of the aperture volume (filled circles, squares, and triangles: 71%, 15; 60%, 15; 53%, 15; and open circles, squares, and triangles: 71%, 20; 60%, 20; 53%, 20; glycerol and PSI, respectively) .

q_ℓ and viscosity η, $V_b \propto P/\eta q_\ell$. This relation is explained in terms of geometrically controlled pinch-off. The pinch-off time is inversely proportional to liquid flow rate, and the gas flow rate q_g is set by viscous drag on the gas thread to be $q_g \propto P/\eta$ due to pushing forward the downstream liquid column of viscosity η. Our measurements of bubble volume confirm the scaling of this relationship, as shown in figure 3*b*.

Garstecki *et al.* (2004) found that frequency of bubble formation f was directly proportional to the flow rate and gas pressure $f \propto P q_\ell$, but our measurements (varying the flow rate with a fixed gas pressure), reported in figure 4*a*, clearly deviate from this linear relationship at high flow rates. This discrepancy can be understood in terms of the extra pressure drop produced in the channel by the flow of liquid through the channel P_c as well as the pressure drop induced by the bubbles in the channel (see figure 5 for a schematic of the notation used). For a rectangular channel with cross-sectional dimensions h and w and length L, the pressure drop for a fluid of viscosity η and flow rate q_ℓ is

$$P_c = \left[\frac{12L}{hw^3 \left[1 - \frac{192}{\pi^5} \sum_{n=0}^{\infty} \frac{1}{(2n+1)^5} \tanh\left(\frac{(2n+1)w\pi}{2h} \right) \right]} \right] \eta q_\ell. \tag{3.1}$$

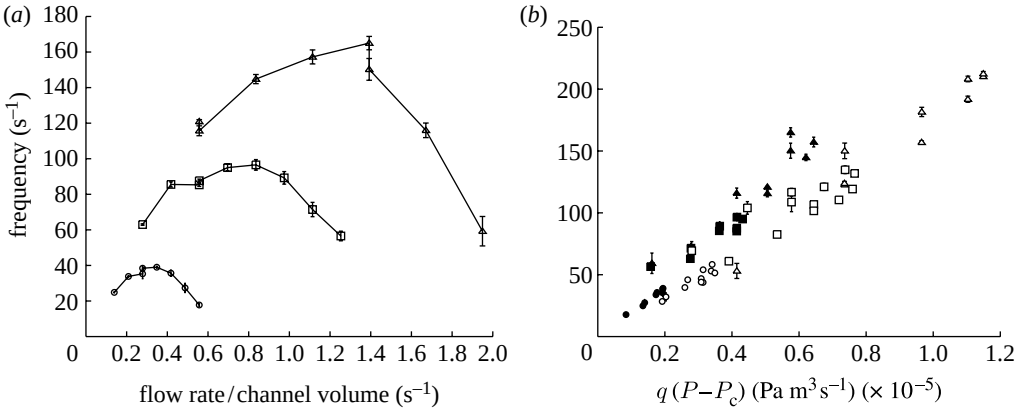

Figure 4. (*a*) Frequency plotted against the applied flow rate for different viscosity solutions at the same gas pressure of 15 PSI. The previously observed scaling $f \propto Pq_\ell$ (adapted from Garstecki *et al.* 2004) is clearly not applicable in this regime, as the frequency relation shows a distinct maximum. For flow rates larger than those presented here, the gas thread is observed to reverse direction and retreat through the gas inlet (glycerol: circles, 71%; squares, 60%; and triangles, 53%). (*b*) The previously observed relation $f \propto q_\ell(P-P_c)$ (Raven *et al.* 2006) collapses observations with different viscosities, but the magnitudes of different datasets depend on the absolute gas pressure. Experiments at gas outlet pressure $P=20$ PSI (open) yield consistently smaller results than experiments at $P=15$ PSI (closed) (filled circles, squares and triangles: 71%, 15; 60%, 15; 53%, 15; and open circles, squares and triangles: 71%, 20; 60%, 20; 53%, 20; glycerol and PSI, respectively).

For simplicity, we rewrite this equation as $P_c = \alpha q_\ell$, where α is the hydrodynamic resistance. Raven *et al.* (2006) extended the frequency relationship to include the channel pressure drop P_c with $f \propto (P-P_c)q_\ell$ for low pressures and $f \propto 1/q_\ell$ for high pressures. This modified relation arises from the two time scales present in bubble formation: the thread pinch-off time, which is proportional to $1/q_\ell$; and the thread growth time, which is observed experimentally to be proportional to $1/(q_\ell(P-P_c))$. Direct measurements of the evolution of gas thread volume (figure 6) confirm the idea that there are two distinct time scales in the thread pinch-off dynamics in our system as well (labelled as a, b in figure 6). There is initially slow volume growth, corresponding to the thread growth up to the flow-focusing constriction followed by a rapid volume increase corresponding to bubble formation and pinch-off in the constriction. In our experiments, the thread growth time is significantly longer than the bubble formation and pinch-off and dominates in determining the frequency of bubble generation. The frequency relation $f \propto q_\ell(P-P_c)$ explains the observed variation for different viscosities and flow rates, but does not capture the dependence on gas inlet pressure P (figure 4*b*).

(*c*) *A model for bubbling frequency*

To move beyond an empirical model for the bubble generation frequency, we must understand what controls the time scale of thread growth. We can model the initial thread growth by a column of gas at fixed pressure P growing into a fluid-filled tube. Neglecting the effects of surface tension and interface shape, a simple force balance sets the flow rate of gas q_g to be $q_g = P/\alpha$, where α is the hydrodynamic resistance of the liquid through the channel. If, in addition to the gas flow, the liquid flows with a volumetric rate q_ℓ, the gas flow rate is reduced to

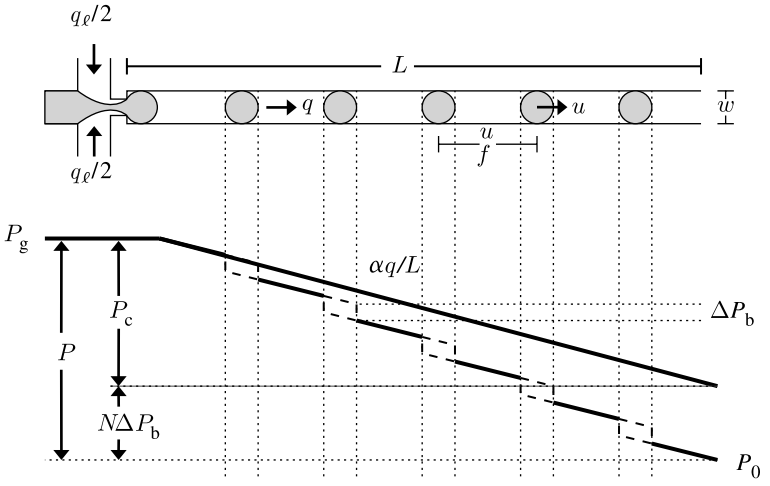

Figure 5. Schematic of the variables used in our model of bubble generation; the pressure throughout the device is plotted below. The outlet channel has length L and width w as shown; the channel height h is not shown in the diagram. Gas at pressure P_g, which is a pressure $P=P_g-P_0$ above the tube outlet, is flowed into a flow-focusing device; the gas has a flow rate q_g. Liquid, with total flow rate q_ℓ, is also flowed into the junction, equally from above and below with flow rates $q_\ell/2$, producing a total flow $q=q_\ell+q_g$. Once the gas thread is sufficiently large, bubbles of volume V_b are formed at a frequency f and are carried by the flow with velocity $u=q/hw$. In steady-state bubble production, this leads to a bubble–bubble separation of u/f and a total number N bubbles in the channel of $N=fL/u$. In pressure drop due to liquid flow P_c is given by $P_c=\alpha q$, where α is the hydrodynamic resistance (equation 3.1). In bubble-free regions, this gives a pressure that drops linearly with slope $\alpha q/L$. In addition to the hydrodynamic pressure drop, each bubble contributes an additional pressure drop $P\Delta_b$, yielding a total bubble contribution of $N\Delta P_b=fLhw\Delta P_b/u$. Force balance requires the imposed pressure difference P to be equal to the total pressure drop, $P=\alpha q+N\Delta P_b$, which sets the gas flow rate.

$q_g=P/\alpha-q_\ell=(P-P_c)/\alpha$, giving a total flow rate $q=q_g+q_\ell$. For the flow-focusing device, the gas can only fill a finite volume, V_f, before the effects of the flow-focusing junction dominate, which sets a time scale for slow growth of $\tau_g=V_f/q_g$. When thread growth dominates bubble generation, this estimate gives a frequency generation of $f=(P-P_c)/\alpha V_f$.

This simple model is in disagreement with the observed scaling of frequency, which depends on both pressure drop and flow rate, and not simply pressure drop (figure 4*b*; Garstecki *et al.* 2004; Raven *et al.* 2006). This discrepancy can be explained by realizing that the observed experimental frequencies correspond to steady bubble trains, not simply fluid-filled channels. As has been observed by Raven & Marmottant (2006) in a foam generator, the bubbles downstream also contribute to the pressure drop in the channel and can dramatically alter the flow behaviour. The total pressure drop ΔP for a steady flow in a channel of length L may then be written as $\Delta P=P-P_c-\sum_i^{x_i<L}\Delta P_{b,i}$, where $\Delta P_{b,i}$ is the additional pressure drop of the ith bubble in the channel. This extension to the model allows the generation frequency to be calculated as

$$f=\frac{\left(P-P_c-\sum_i^{x_i<L}\Delta P_{b,i}\right)}{\alpha V_f}. \tag{3.2}$$

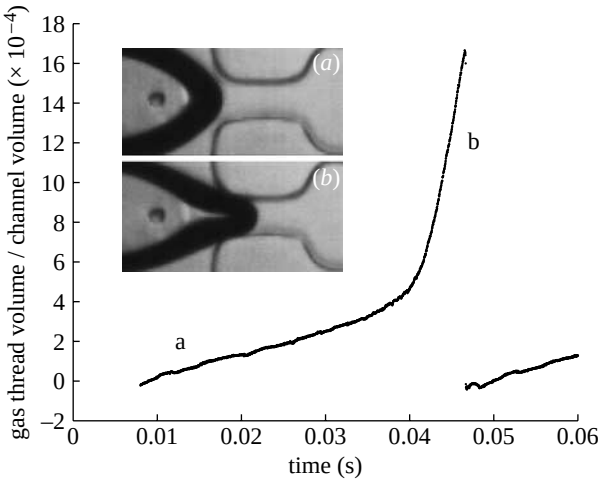

Figure 6. The volume of the gas thread as the gas stream undergoes steady-state bubble pinch-off. There are three distinct regimes seen in the evolution of the volume of the gas thread: (*a*) slow initial growth from outlet to constriction and (*b*) fast bubble growth into the outlet and finally pinch-off and retraction. The initial growth is the slowest step in our experiments and is dominant in setting the generation frequency. The fast bubble growth corresponds to the largest volume increase, however, and thus sets the final bubble volume.

If the stream is assumed to be in a single period, steady-state mode, the sum in equation (3.2) can be replaced by $N\Delta P_{\mathrm{b}}$, where each of the N bubbles contributes the same pressure drop ΔP_{b}. The bubble velocity is proportional to the average fluid velocity, so for a channel of height h, width w and length L, the total number of bubbles, N, in the channel is $N=fLhw/q_\ell$. Combining the modified pressure drop from a stream of steady bubbles with the simple model for frequency yields a relation for the steady-state generation frequency

$$f_0 = \frac{\alpha q_\ell (P - P_{\mathrm{c}})}{\alpha q_\ell V_{\mathrm{t}} + V_{\mathrm{c}} \Delta P_{\mathrm{b}}}, \tag{3.3}$$

where $V_{\mathrm{c}}=Lhw$ is the volume of the channel. In the limit that $q_\ell \ll V_{\mathrm{c}}\Delta P_{\mathrm{b}}/\alpha V_{\mathrm{t}}$, equation (3.3) can be well approximated by $f_0=q_\ell(P-P_{\mathrm{c}})/V_{\mathrm{c}}\Delta P_{\mathrm{b}}$.

A general relation for the pressure drop across a bubble ΔP_{b}, for a bubble comparable in size to the channel width in a rectangular channel is not known to us. Feurstman *et al.* (2007) determined a relation for ΔP_{b} for bubbles long compared to the channel width in rectangular channels that depends on the bubble length, liquid flow rate and surface tension. Adzima & Velankar (2006) likewise found a relation for liquid droplets in a liquid–liquid flow. The pressure drop of the bubble should depend on size, velocity, viscosity and surface tension of the bubble and viscosity and flow rate of the fluid. As the viscosity of air is small enough to neglect and the surface tension is similar for all of our experiments, we expect the observed ΔP_{b} behaviour to be dominated by bubble velocity and size effects. We do not have a direct measurement of the additional pressure drop due to a bubble, but we can invert equation (3.3) to arrive at an estimate of ΔP_{b}. This step yields, in the limit of small q_ℓ, $\Delta P_{\mathrm{b}}=q_\ell(P-P_{\mathrm{c}})/f_0 V_{\mathrm{c}}$, giving ΔP_{b} in terms of properties that have been experimentally measured. We

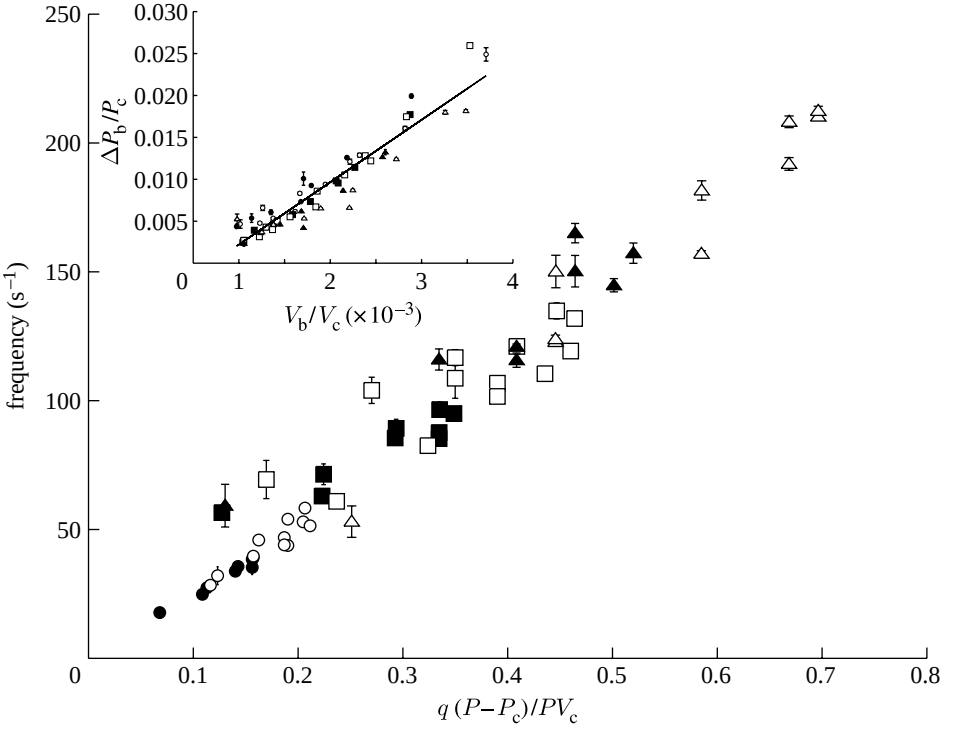

Figure 7. Using the approximate relationship for excess pressure drop due to a bubble $\Delta P_b = q_\ell(P-P_c)/f_0 V_c$ allows us to approximate the pressure drop across a bubble ΔP_b. Physical arguments suggest that ΔP_b is linearly proportional to the channel pressure drop P_c, so we normalize by this quantity to provide an estimate of the dependence of ΔP_b on bubble volume V_b, as shown in the inset. There is an approximate linear dependence on V_b, so we make the approximation $\Delta P_b = \psi P_c V_b/V_c$, where ψ is a dimensionless constant, equal to approximately 7 in our experiments. This yields the final scaling relationship for frequency, $f \propto q_\ell(P-P_c)/PV_c$, which collapses all of the data from experiments on a single channel geometry using different viscosities, pressures and flow rates as shown in the main figure (filled circles, squares, and triangles: 71%, 15; 60%, 15; 53%, 15; and open circles, squares, and triangles: 71%, 20; 60%, 20; 53%, 20; glycerol and PSI, respectively).

expect the pressure drop to be proportional to the viscosity and liquid flow rate, which is itself proportional to P_c, so a plot of our experimental ΔP_b estimate normalized by P_c should yield the bubble volume dependence of ΔP_b (figure 7). The data are approximately linear with V_b, which allows us to make the empirical approximation $\Delta P_b = \psi P_c V_b/V_c$, where the dimensionless proportionality constant ψ depends on surface tension and channel geometry.

The final piece to clarifying the scaling relation for frequency is the relation for volume scaling found by Garstecki *et al.* (2004), $V_b = V_t P/P_c$, where V_t is the proportionality constant in the volume relation (figure 3*b*). Thus, the pressure drop can be rewritten as $\Delta P_b = \psi P V_t/V_c$. The final approximate relation for frequency becomes

$$f_0 = q_\ell(P - P_c)/\psi V_t P. \tag{3.4}$$

This relation agrees well with our measurements over a range of pressures, flow rates and viscosities (figure 7).

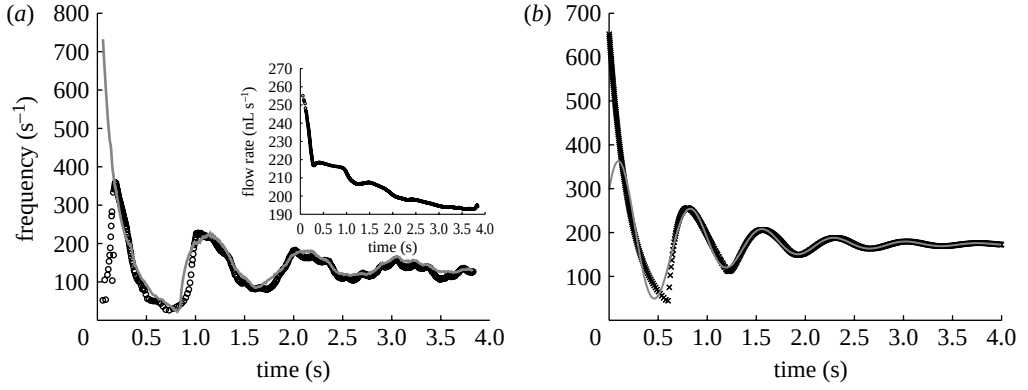

Figure 8. (*a*) Measurement of bubble frequency for start up of a flow-focusing device. The channel is initially emptied of bubbles by increasing the liquid flow rate to drive the gas stream backwards. On lowering the flow rate to the desired value, the bubble frequency shows distinct oscillations. Simple numerical models (see text) based on the relationship between frequency and total pressure drop can be used to reproduce the observed oscillations (circles, calculated frequency; solid grey line, measured frequency). The inset shows the estimated mean flow rate that is not directly set by the syringe pump due to system compressibility. (*b*) Comparison of numerical and analytical results for a model bubble generation start up. The analytical model provides the oscillation frequency and decay exponent—the amplitude and phase are simply fit to the numerical values. The analytical model does not account for velocity fluctuations, so an intermediate flow rate has been used (crosses, numerical result; solid grey line, analytical result).

4. Unsteady bubble generation

One experimental test of the role of feedback in the bubble generation frequency is to measure this frequency with varying numbers of bubbles in the outlet channel. This test can be practically accomplished by measuring the start-up behaviour of an initially bubble-free channel. To this end, measurements of a start-up period were taken by raising the liquid velocity above the rate at which the gas thread retreats from the outlet and, once the device is cleared of bubbles, lowering the flow rate to the desired value.

The start-up behaviour of a flow-focusing device from such an experiment is presented in figure 8*a*. The frequency of bubbles during start up oscillates from an initially high value and then slowly settles towards a stable generation frequency. One unexpected feature of the measurement is an initial increase in the bubble generation frequency, as one might have expected bubbles to increase the flow-generated pressure and thus decrease the frequency. This feature can be understood by looking at the average bubble velocity during generation (figure 8*a*), where it is seen that the liquid flow rate decreases slowly from an initially large value. This fluctuation is due to compressibility in the syringe—most likely owing to trapped small air bubbles.

A numerical model can be developed to predict the time behaviour of a flow-focusing junction attached to a single outlet channel. The model is based on generating bubbles at a frequency dictated by equation (3.2). These bubbles are then carried by the flow at the mean flow velocity u until they reach the end of the channel. With the positions of all of the bubbles in the channel, the total

pressure drop can be calculated to yield the new generation frequency. This process is then iterated to determine the temporal behaviour of the system. When taking into account the variable flow rate caused by compressibility of the system, the model does a reasonable job of replicating the observed oscillations (figure 8*a*).

The numerical model lends itself to an analytical approximation. When the number of bubbles in the channel is large, it is reasonable to approximate the discrete bubbles by a continuous density of bubbles $\rho(x)$, i.e. the number per length. For bubbles moving at a constant velocity u, there is a simple relation between a continuous frequency $f(t)$ and density, namely $\rho(x)=f(t-x/u)/u$. Similarly, the total pressure drop due to bubbles in the channel of length L can be calculated as $\Delta P_{\mathrm{bubble}} = \int_0^L \rho(x)\,\mathrm{d}x$. Combining these elements, we arrive at a continuous equation for the generation frequency

$$f(t) = \frac{\left(P - P_{\mathrm{c}} - \Delta P_{\mathrm{b}} \int_{t-L/u}^{t} f(t)\,\mathrm{d}t\right)}{\alpha V_{\mathrm{t}}}. \tag{4.1}$$

In addition to the steady-state solution, one analytical solution to this integral equation is an offset decaying exponential $f=f_0+A\mathrm{e}^{(\mathrm{i}-\Delta)\omega t}$. Substituting this function in equation (4.1), one finds that f_0 is the steady-state solution for frequency, given in equation (3.4). There is also a particular set of solutions for ω and Δ given by

$$\beta \sin(\omega t_0) = \omega \exp(\beta t_0 - \omega t_0 \cot(\omega t_0)), \tag{4.2}$$

$$\Delta = \frac{\log(\beta \sin(\omega t_0)/\omega)}{\omega t_0}, \tag{4.3}$$

where $t_0=L/u$ is the bubble travel time through the channel and $\beta=\Delta P_{\mathrm{b}}/\alpha V_{\mathrm{t}}$. The amplitude A of frequency oscillations is a free parameter and must be set by the initial conditions.

The frequencies that satisfy equation (4.3) form a family of solutions to the bubble oscillation problem. The smallest exponential decay—corresponding to the longest lived solution—occurs for the smallest non-zero value of ω. Comparing this solution with the numerical solution for bubble start up shows a strong agreement after the initial decay (figure 8*b*). The initial discrepancy is most likely due to the initially empty starting conditions in the numerical simulation. The agreement between the numerical and the analytical models exists until the number of bubbles in the channel becomes small, at which point the underlying assumption that the bubbles can be treated continuously is no longer valid.

5. Conclusions

We have furthered the understanding of the generation frequency behaviour in a microfluidic flow-focusing bubble generator. Frequency is controlled by two time scales—the time taken for a thread to fill the flow-focusing constriction and the time required for the thread to pinch-off to form a bubble. The growth time is controlled by the pressure difference between the gas thread and the surrounding liquid, which in turn is controlled by the liquid flow rate and the density of

bubbles downstream from the constriction. For steady-state bubble production, the frequency of bubble production can be approximated by $f \propto q_\ell (P - P_c)/P$, which is similar to experimental results obtained by others.

For single flow-focusing devices, downstream effects are most important when the flow is pressure driven, as the channel flow primarily affects the absolute upstream pressure. In geometrically controlled flow-focusing devices, this feedback stabilizes the flow—increased bubble production increases the channel resistance, which in turn lowers the bubble production rate. The negative feedback in the channels damps frequency transients. For massively parallel devices, however, these feedback effects become important even for flow rate driven devices, as these would typically be supplied from a single syringe pump. This manner of forcing would cause the flow rate at a particular junction to be set by the resistance through the entire parallel arm, so that device feedback can have a pronounced effect, as seen by Barbier *et al.* (2006), even when all components of the system are incompressible. In designing parallel devices for monodisperse foam and emulsion formation, care must be taken to mitigate the downstream effects of bubbles or droplets on flow, especially at channel junctions (see Engl *et al.* 2005; Jousse *et al.* 2006). Feedback, even in parallel systems, need not be simply a liability in the operation of microfluidic devices. For example, Prakash & Gershenfeld (2007) have taken advantage of the nonlinear interactions at channel junctions to produce a variety of microfluidic logic operations and oscillators. The nonlinear operation of multiphase flow generators might be similarly leveraged.

We would like to acknowledge the support from the Harvard MRSEC (DMR-0213805) and the Schlumberger Future of Research programme.

References

Adzima, B. J. & Velankar, S. S. 2006 Pressure drops for droplet flows in microfluidic channels. *J. Micromech. Microeng.* **16**, 1504–1510. (doi:10.1088/0960-1317/16/8/010)

Anna, S. L. & Mayer, H. C. 2006 Microscale tipstreaming in a microfluidic flow focusing device. *Phys. Fluids* **18**, 121 512. (doi:10.1063/1.2397023)

Anna, S. L., Bontoux, N. & Stone, H. A. 2003 Formation of dispersions using 'flow focusing' in microchannels. *Appl. Phys. Lett.* **82**, 364–366. (doi:10.1063/1.1537519)

Barbier, V., Willaime, H., Tabeling, P. & Jousse, F. 2006 Producing droplets in parallel microfluidic systems. *Phys. Rev. E.* **74**, 046 306. (doi:10.1103/PhysRevE.74.046306)

Beebe, D. J., Mensing, G. A. & Walker, G. M. 2002 Physics and applications of microfluidics in biology. *Annu. Rev. Biomed. Eng.* **4**, 261–286. (doi:10.1146/annurev.bioeng.4.112601.125916)

Bretherton, F. P. 1961 The motion of long bubbles in tubes. *J. Fluid Mech.* **10**, 166–188. (doi:10.1017/S0022112061000160)

Duffy, D. C., McDonald, J. C., Schueller, O. J. A. & Whitesides, G. M. 1998 Rapid prototyping of microfluidic systems in poly(dimethylsiloxane). *Anal. Chem.* **70**, 4974–4984. (doi:10.1021/ac980656z)

Engl, W., Roche, M., Colin, A., Panizza, P. & Ajdari, A. 2005 Droplet traffic at a simple junction at low capillary numbers. *Phys. Rev. Lett.* **95**, 208 304. (doi:10.1103/PhysRevLett.95.208304)

Eggers, J. 1993 Universal pinching of 3D axisymmetric free-surface flow. *Phys. Rev. Lett.* **71**, 3458–3460. (doi:10.1103/PhysRevLett.71.3458)

Eggers, J. 1997 Nonlinear dynamics and breakup of free-surface flows. *Rev. Mod. Phys.* **69**, 855–929. (doi:10.1103/RevModPhys.69.865)

Fuerstman, M. J., Lai, A., Thurlow, M. E., Shevkoplyas, S. S., Stone, H. A. & Whitesides, G. M. 2007 The pressure drop along rectangular microchannels containing bubbles. *Lab Chip* **7**, 1479–1489. (doi:10.1039/b706549c)

Ganan-Calvo, A. M. & Gordillo, J. M. 2001 Perfectly monodisperse microbubbling by capillary flow focusing. *Phys. Rev. Lett.* **87**, 274 501. (doi:10.1103/PhysRevLett.87.274501)

Garstecki, P., Gitlin, I., DiLuzio, W., Whitesides, G. M., Kumacheva, E. & Stone, H. A. 2004 Formation of monodisperse bubbles in a microfluidic flow-focusing device. *Appl. Phys. Lett.* **85**, 2649–2651. (doi:10.1063/1.1796526)

Garstecki, P., Stone, H. A. & Whitesides, G. M. 2005 Mechanism for flow-rate controlled breakup in confined geometries: a route to monodisperse emulsions. *Phys. Rev. Lett.* **94**, 164 501. (doi:10.1103/PhysRevLett.94.164501)

Garstecki, P., Fuerstman, M. J., Stone, H. A. & Whitesides, G. M. 2006 Formation of droplets and bubbles in a microfluidic T-junction—scaling and mechanism of break-up. *Lab Chip* **6**, 437–446. (doi:10.1039/b510841a)

Jensen, M. J., Stone, H. A. & Bruus, H. 2006 A numerical study of two-phase Stokes flow in an axisymmetric flow-focusing device. *Phys. Fluids* **18**, 077 103. (doi:10.1063/1.2214461)

Jousse, F., Farr, R., Link, D. R., Fuerstman, M. J. & Garstecki, P. 2006 Bifurcation of droplet flows within capillaries. *Phys. Rev. E* **74**, 036 311. (doi:10.1103/PhysRevE.74.036311)

Lord Rayleigh 1879 On the capillary phenomena of jets. *Proc. R. Soc. Lond.* **29**, 71–97. (doi:10.1098/rspl.1879.0015)

Okushima, S., Nisisako, T., Torii, T. & Higuchi, T. 2004 Controlled production of monodisperse double emulsions by two-step droplet breakup in microfluidic devices. *Langmuir* **20**, 9905–9908. (doi:10.1021/la0480336)

Plateau, J. 1849 Statique experimentale et theorique des liquides soumis aux seules forces moleculaires. *Acad. Sci. Brux. Mem.* **23**, 5.

Prakash, M. & Gershenfeld, N. 2007 Microfluidic bubble logic. *Science* **315**, 832–835. (doi:10.1126/science.1136907)

Raven, J. P. & Marmottant, P. 2006 Periodic microfluidic bubbling oscillator: Insight into the stability of two-phase microflows. *Phys. Rev. Lett.* **97**, 154 501. (doi:10.1103/PhysRevLett.97.154501)

Raven, J. P., Marmottant, P. & Graner, E. 2006 Dry microfoams: formation and flow in a confined channel. *Eur. Phys. J. B* **51**, 137–143. (doi:10.1140/epjb/e2006-00197-6)

Thorsen, T., Roberts, R. W., Arnold, F. H. & Quake, S. R. 2001 Dynamic pattern formation in a vesicle-generating microfluidic device. *Phys. Rev. Lett.* **86**, 4163–4166. (doi:10.1103/PhysRevLett.86.4163)

Umbanhowar, P. B., Prasad, V. & Weitz, D. A. 2000 Monodisperse emulsion generation via drop break off in a coflowing stream. *Langmuir* **16**, 347–351. (doi:10.1021/la990101e)

Utada, A. S., Lorenceau, E., Link, D. R., Kaplan, P. D., Stone, H. A. & Weitz, D. A. 2005 Monodisperse double emulsions generated from a microcapillary device. *Science* **308**, 537–541. (doi:10.1126/science.1109164)

Utada, A. S., Fernandes-Nieves, A. F., Stone, H. A. & Weitz, D. A. 2007 Dripping to jetting transitions in coflowing liquid streams. *Phys. Rev. Lett.* **99**, 094 502. (doi:10.1103/PhysRevLett.99.094502)

Wong, H., Radke, C. J. & Morris, S. 1995 The motion of long bubbles in polygonal capillaries I thin films. *J. Fluid Mech.* **292**, 71–94. (doi:10.1017/S0022112095001443)